AMSI VACATION RESEARCH SCHOLARSHIPS 2019–20

EXPLORE THE MATHEMATICAL SCIENCES THIS SUMMER

Bragg Edge

Neutron Strain Tomography

Thomas Vandenberg

Supervised by Associate Professor Mike Meylan

University of Newcastle

Vacation Research Scholarships are funded jointly by the Department of Education and Training and the Australian Mathematical Sciences Institute.

AMSI AUSTRALIAN MATHEMATICAL SCIENCES INSTITUTE

Australian Government Department of Education

Abstract

Non-destructive strain imaging of polycrystalline materials may be achieved by analysing energy and spatially resolved transmission data of a cold neutron beam. Time of flight spectroscopy is utilised to determine the wavelength position of Bragg edges in the transmission data, and from this information the average lattice spacing for a particular lattice plane along a path through the material may be determined. Data from a spallation neutron source in Japan was examined, and Bragg edge images created using an unconventional method. From this, averaged lattice spacing and strain images were created.

1 Introduction

Strain imaging of poly-crystalline materials has been achieved using a number of techniques, such as electron back-scatter diffraction and X-ray diffraction, however these methods are usually limited to surface analysis due to interactions with electrons in the material reducing penetrating power of the probe particles [3].

The use of neutrons in Bragg edge strain tomography presents an exciting opportunity to image inner features without having to remove parts of the sample, allowing non-destructive analysis of characteristics such as strain within a material.

1.1 Neutron Physics

The neutron was discovered in 1932 by James Chadwick, and has since been utilised in a diverse range of applications. The reason that this non-destructive analysis can be achieved using neutrons is due to the nature of neutron interactions with the material. Consisting of a single up quark and two down quarks, neutrons have no net charge, and do not interact significantly with electrons surrounding atomic nuclei in the poly-crystalline material.

There is some significant interaction between the neutrons and the atoms in the material, otherwise no information would be gained from the transmission spectrum. This interaction occurs between the nucleus of the atoms in the material and the passing neutrons. Neutrons display much higher penetrating power than particles which interact significantly with electrons in the material, owing to the relative radial size of the nucleus compared to the electron cloud. This allows neutrons to travel much further through the lattice without interacting with the material and being scattered or absorbed, while photons and electrons interact with the electron cloud and are more likely knocked off course.

Hence, a beam of neutrons passing through the bulk sample of poly-crystalline material can maintain sufficient intensity to be detected after leaving and display information about their particular pathway through that material.

1.1.1 Generation of Neutron Beam

The neutrons required to carry out this imaging technique can be produced by fission reactions in a nuclear reactor, however spallation neutron sources are more suited to producing the required pulsed beams for strain imaging. This involves accelerating protons in a particle accelerator and directing them toward a target material, such as lead, whose nuclei are excited when impacted by the high energy protons. In the process of relaxation, about 20 neutrons are released per nucleus. These neutrons are cooled in a moderator, such as liquid hydrogen, ready to be used for a variety of research interests.

1.1.2 Neutron Wavelength

In 1924, Louis de Broglie proposed that since photons had been shown to exhibit both wave and particle characteristics, then perhaps other matter classically thought as being 'particle-like' could exhibit wave properties.

The de Broglie wavelength is given by [4]

$$\lambda = \frac{h}{p} \tag{1}$$

Where p is the momentum of the particle and λ is the wavelength of the wave associated with the particle, while h is Planck's constant. This idea was supported by results from an experiment performed by Clinton Davisson and Lester Germer, which involved studying the diffraction pattern of electrons scattered by the surface of a sample of nickel metal [7].

The dependence of the wavelength of a neutron on its momentum is central to Bragg edge neutron strain tomography. 'Cold' neutrons, with wavelengths of the order of $1\mathring{A}$, are used so that their corresponding wavelength is approximately equal to lattice spacing, so that Bragg edges can be observed.

1.1.3 Neutron Detection

Gas ionisation detectors count neutron incidences by inducing an avalanche of charged particles when a neutron enters the device, which is detected as a current. They provide little information on the energy of the incident neutron. Energy resolution comes from the application of time of flight spectroscopy.

1.2 Bragg Edge

1.2.1 Bragg Condition

In 1913, William Henry Bragg and his son, William Lawrence Bragg, showed that X-rays incident on an atomic lattice could be coherently scattered if the incoming radiation satisfied the condition now known as the 'Bragg Law' [5],

$$n\lambda = 2d_{hkl}sin(\theta) \tag{2}$$

Where λ is the wavelength of the incoming waves, d_{hkl} is the lattice spacing for a particular [h,k,l] lattice plane, θ is the angle of incidence (between incoming waves and the crystallographic plane) and $n \in \mathbb{N}$.

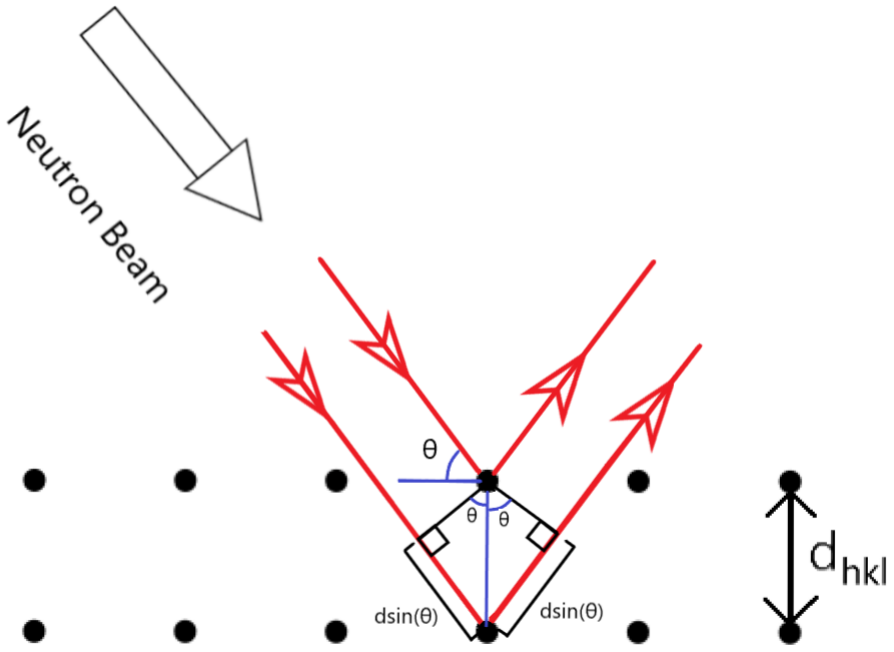

Figure 1: Bragg Law Visual Representation

If this condition is satisfied, the wave-fronts which are reflected from neighbouring [h,k,l] lattice planes recombine in phase for certain angles of reflection, resulting in constructive interference, as can be seen in Figure 1.

1.2.2 Time of Flight Spectroscopy

From Equation 1 we see that neutron wavelength varies with momentum. The momentum of a neutron is given by [8]

$$p = \frac{m_0 v}{\sqrt{1 - \frac{v^2}{c^2}}}$$

Where m_0 is the rest mass of the neutron, v is its velocity and c is the speed of light.
The neutrons used in Bragg edge strain tomography have velocities of approximately 2000 ms^{-1}, less than one hundred thousandth of the speed of light. Therefore, the effect of mass dilation is negligible and so momentum for these velocities can be approximated using the classical formula,

$$p \approx m_0 v$$

Hence, substituting into Equation 1, for non-relativistic velocities ($v \ll c$),

$$\lambda \approx \frac{h}{m_0 v} \tag{3}$$

Therefore, within the generated neutron beam, which contains a spectrum of neutron velocities, there will exist a distribution of neutron wavelengths. The time taken for a neutron to reach the detector from the beam generator is used to determine the velocity of the neutron. This velocity can be converted to wavelength using Equation 3.

The distance travelled by the neutrons between the beam chopper and the detector is crucial in separating the velocity components of the beam to increase wavelength resolution.

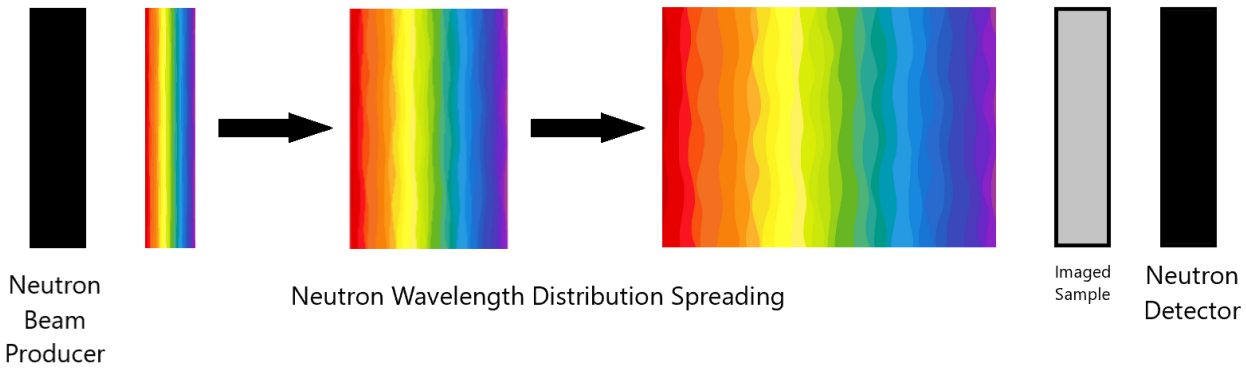

Figure 2: Neutron beam containing different velocity components, and hence wavelength components (see Equation 3)

1.2.3 Transmission Increase at Bragg Edge

If a poly-chromatic beam of neutrons, with wavelengths approximately equal to a particular lattice plane spacing present in the sample to be probed, is incident on this periodic collection of atoms, then only some of the wavelength components will be Bragg scattered.

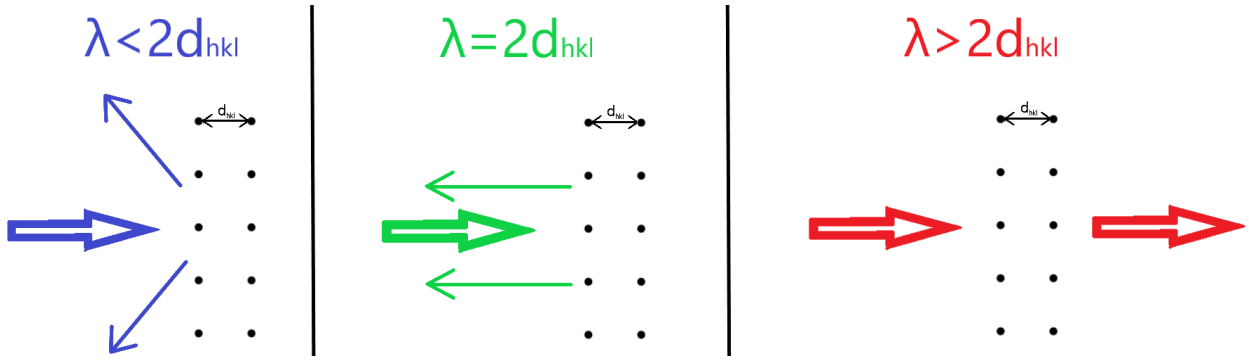

Figure 3: Bragg edge transmission intensity increase

This is because for Bragg scattering to occur, the incident wave must satisfy the Bragg condition (Equation 2). Now, if we assume that the substance is made up of a mosaic arrangement of lattice structures (poly-crystalline), with each orientation occurring with approximately the same frequency throughout the sample, then for neutron wavelengths less than $2d_{hkl}$, there will be orientations of collections of this crystallographic plane which cause the incident beam to undergo Bragg reflection.

As time passes by, the wavelength of neutrons incident on the sample gradually increases due to the nature of the time of flight beam setup, however no significant change in the total transmission intensity is observed, since as one particular orientation is no longer able to Bragg reflect, another orientation (occurring with the same frequency) more suited to this new longer wavelength takes its place in the attenuation scheme.

However, when the wavelength of the incident neutrons reaches $2d_{hkl}$, only perpendicular orientations of this particular plane to the incoming neutron beam are able to induce Bragg scattering.

And then, as soon as the incident neutron wavelength exceeds $2d_{hkl}$, no orientation of this particular crystallographic plane, with spacing d_{hkl} is able to fulfill the Bragg condition. This is because $|sin(\theta)| \leq 1$ for all $\theta \in [0, 2\pi]$, so if the neutron wavelength exceeds twice the lattice spacing, $\lambda > 2d_{hkl}$, then no orientation of lattice planes with spacing d_{hkl} can satisfy Equation 2, and hence Bragg scattering can not occur from these planes. This results in a sudden increase in the transmission of neutrons through the material, known as a Bragg edge.

Sharp increases in the neutron transmission data as a function of wavelength, and hence also as a function of time of arrival at the detector, are observed due to this phenomenon. At the point where the neutron wavelength exceeds twice the lattice spacing, $\lambda = 2d_{hkl}$, neutron transmission through the material increases dramatically since Bragg back-scattering from that particular lattice plane is no longer contributing. Using this knowledge, the appearance of Bragg edges in transmission data can be utilised to probe the inner properties of the imaged material.

So, Bragg edges will be observed in the transmission spectrum over time for each pixel, corresponding to different lattice plane spacings present in the polycrystalline material. While theoretically they should be observed as a step function, equipment uncertainties and other factors result in the 'smearing out' of the observed Bragg edge.

One approach of detecting the time of flight point corresponding to the centre of a Bragg edge is to fit an appropriate function to the data, such as Equation 4. This equation provides an accurate approximation of the Bragg edge shape observed in neutron time of flight transmission data. It is fit to Bragg edge data using a least squares minimisation process to approximate values for each parameter. Most importantly, from this fit, a value for the time of flight corresponding to the 'centre' of the Bragg edge is obtained. [1]

$$\text{Transmission(t)}=\text{e}^{-nw\sigma_0}\left[e^{-nw\sigma_{hkl}}+(1-e^{-nw\sigma_{hkl}})\times\frac{1}{2}\left[erfc(-\frac{t-t_{hkl}}{\sqrt{2}\sigma})-e^{-\frac{t-t_{hkl}}{\tau}+\frac{\sigma^2}{2\tau^2}}\times erfc(-\frac{t-t_{hkl}}{\sqrt{2}\sigma}+\frac{\sigma}{\tau})\right]\right] \quad (4)$$

Given the Bragg edge time of flight value, obtained from fitting this function to the transmission data, the 'average' lattice plane spacing along the beam path through the sample can be determined for the plane in question.

Let L be the distance travelled by a neutron in the time TOF, so that

$$v = \frac{L}{TOF}$$

Hence, from Equation 3, we have

$$\lambda \approx \frac{h}{m_0 v} = \frac{h}{m_0 L} TOF$$

Now, at the Bragg edge, we know that

$$\lambda = 2d_{hkl}$$

Hence, combining these yields

$$d_{hkl} = \frac{h}{2m_0 L} TOF_{BraggEdge} \quad (5)$$

A linear relationship connects the neutron time of flight value at the Bragg edge to the average lattice spacing along the neutron beam path.

1.3 Strain

It turns out that the measured lattice spacing using Equation 5, d_{hkl}, is only an average along that particular neutron beam path. This is due to stresses within (residual stress) and external stresses acting on the material, causing some atoms in the substance to shift from their equilibrium position. This shift results in a change in the measured plane spacing for a particular lattice plane occurring along that beam path, observed as a shift in the Bragg edge position. Hence, shifts in the position of Bragg edges from the d_0 unstrained spacing indicate strain in the polycrystalline material along that path.

Strain, ε, is defined as

$$\varepsilon = \frac{d - d_0}{d_0}$$

where d is the measured 'average' lattice plane spacing along the particular path and d_0 is the unstrained spacing corresponding to that lattice plane.

1.4 Longitudinal Ray Transform

Strain at each point in the material is described by the strain tensor. Different stresses can be present along each path, and hence strains will differ along any particular path, resulting in this 'averaging' of lattice spacings contributing to the final measured Bragg edge position. The contribution of stresses along each path is described by the Longitudinal Ray Transform. I_ε is the observed 'averaged' strain for a particular path, determined from the Bragg edge position. [9]

$$I_\varepsilon = \int_0^L \hat{n}^T \varepsilon(x_0 + s\hat{n})\hat{n}\, ds$$

The projection of the strain in the direction of beam propagation, $\hat{n}$, is summed over the path through the material to produce the measured strain value, which is obtained from the Bragg edge position. Using this knowledge, we can attempt to tomographically reconstruct the strain tensor field in the material by taking many strain images from different angles.

2 Statement of Authorship

My supervisor thought that it might be interesting to investigate another method of detecting the centre of these Bragg edges present in the data, different to the established function fit method.

He suggested a method which involved applying a convolution including a Gaussian function to the derivative of the data, with the hope that this would pick out the central time of flight point for

each Bragg edge. This would then be used to construct average lattice spacing cross section images.

I wrote Matlab code to interpret experimental data using the convolution method and created cross section images of average lattice spacing and strain through the samples based on this analysis.

3 Convolution

In order to determine the centre of the Bragg edges amongst the noisy signal, the following convolution was applied to the numerical derivative of the raw transmission intensity data as a function of time of flight for each pixel.

$$g(y) = \int_{-\infty}^{\infty} e^{-(\frac{x-y}{a})^2} f'(x)dx \tag{6}$$

Here, $f'(x)$ is the derivative of the neutron transmission intensity data with respect to the time of flight, and a determines the width of the Gaussian function, such that the variance is given by $\sigma^2 = \frac{a}{2}$.

Integrating by parts,

$$\int_{-\infty}^{\infty} e^{-(\frac{x-y}{a})^2} f'(x)dx = \left[e^{-(\frac{x-y}{a})^2} f(x)\right]_{-\infty}^{\infty} - \int_{-\infty}^{\infty} -2\left(\frac{x-y}{a^2}\right) e^{-(\frac{x-y}{a})^2} f(x)dx$$

$$= \left[e^{-(\frac{x-y}{a})^2} f(x)\right]_{-\infty}^{\infty} + \int_{-\infty}^{\infty} 2\left(\frac{x-y}{a^2}\right) e^{-(\frac{x-y}{a})^2} f(x)dx$$

And since

$$\left[e^{-(\frac{x-y}{a})^2} f(x)\right]_{-\infty}^{\infty} = 0$$

We arrive at

$$\int_{-\infty}^{\infty} e^{-(\frac{x-y}{a})^2} f'(x)dx = \int_{-\infty}^{\infty} 2\left(\frac{x-y}{a^2}\right) e^{-(\frac{x-y}{a})^2} f(x)dx$$

Where $f(x)$ is the transmission intensity signal for each pixel as a function of the time of flight to the detector.

So, we have two equivalent convolutions, one which takes the derivative of the data as an input, and the other which utilises the raw transmission data. It is important to remember that while the two methods have been shown to be equivalent, it was assumed that $f(x)$ and $f'(x)$ were continuous functions to prove this, while the data from the detector is discrete in nature. This will be addressed later in the report, where the impact of the discretisation on the difference between the output of each convolution will be examined.

Since the integrand is zero outside the recorded time of flight range, the integral bounds can be reduced to the domain of the time of flight recordings.

4 Interpreting Experimental Neutron Transmission Data Cube from J-PARC Instrument

Experimental neutron transmission data from the 'Energy Resolved Neutron Imaging System' at the Japan Proton Accelerator Research Complex was examined using this convolution method. The data involved a time of flight neutron transmission spectrum for each detector in a 512×512 pixel array. Two data sets were analysed, one for a sample which had very little strain present, and another which exhibited variable strain across the sample.

'Raw' neutron transmission data is shown in Figure 4.

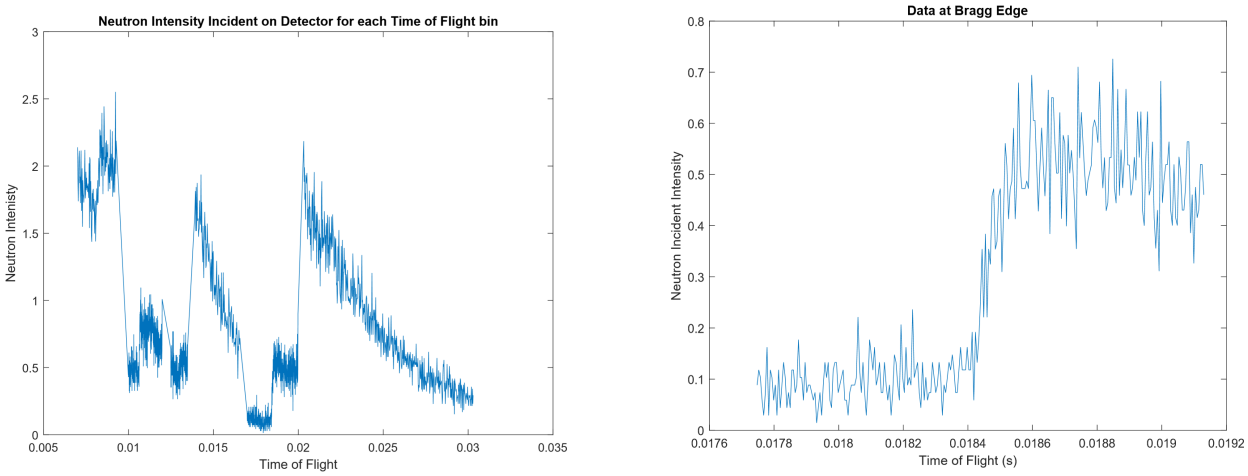

Figure 4: Left - Neutron transmission intensity against time of flight for a single pixel
Right - Zoom on one of the Bragg edges from the transmission data

This is the relative transmission spectrum of the neutron beam through the unstrained sample of polycrystalline material for a single pixel taken from the data cube. Along the horizontal axis are the time of flight detection time bins, which can be linearly converted to corresponding neutron wavelength values using Equation 5. The height of the function at each point is the relative intensity of the transmitted neutron beam at that time point.

It is worth noting that the largest increases in the transmission spectrum, seen in the left plot of Figure 4, are not Bragg edges, but rather data artefacts present due to the nature with which the time of flight bin sizes change at some time points. The Bragg edges are the smaller increases in the transmission spectrum, in between the large discontinuities. A close up view of the Bragg edge which was examined is provided on the right hand side of Figure 4.

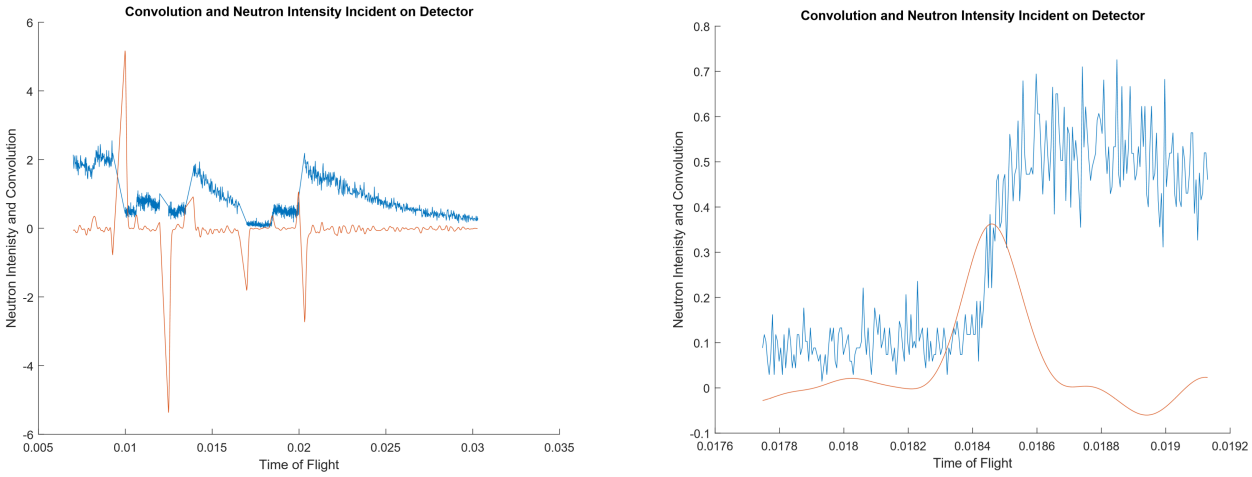

Figure 5: Left - Convolution (orange) applied to neutron transmission intensity spectrum (blue) Right - Zoom on one of the Bragg edges with the convolution applied

When the convolution (orange line) is applied to the whole transmission data set (blue line) for a given pixel, as can be seen on the left in Figure 5, the convolution is observed to be effective in smoothing out the noisy data, and is peaked where the data has a sustained increase or decrease in transmitted intensity. Jumps in the data height due to statistical variation are averaged out by the convolution, and peaks occur at Bragg edges and at the data artefacts. Since the locations of the data artefacts are known based on the experimental setup, they can be subtracted from the resulting set of possible Bragg edge positions detected using the convolution.

The application of the convolution to the whole time of flight data set for each pixel presents the opportunity to find the Bragg edges in the transmission spectrum, as we can calculate the convolution for the whole intensity distribution and then 'look' for peaks. This is not possible with the established function fit technique, since it only fits the data in a small range surrounding the Bragg edge, and so Bragg edges must be searched for manually in the transmission data (if their position is not already known).

The plot on the right in Figure 5 is a close-up look at the convolution in the vicinity of a Bragg edge. The noise is significantly reduced by the convolution, and its peak is in the centre of the Bragg edge jump in neutron transmission.

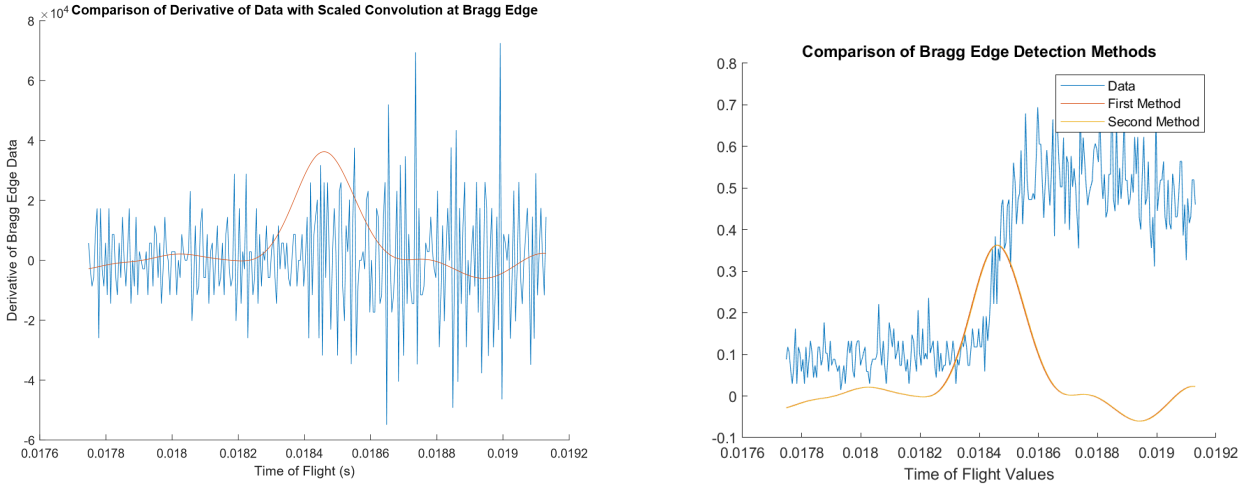

Figure 6: Left - Convolution applied to numerical derivative of neutron transmission intensity spectrum at Bragg edge. Right - Comparison of the two convolution methods, one using the raw data and the other using the derivative of the intensity spectrum.

The two convolution methods, shown earlier to be equivalent if the input function was continuous, are compared in the right plot of Figure 6 when applied to the discrete transmission data. It was observed that their outputs were effectively equivalent, meaning that the choice of whether to use the raw data input or derivative input convolution could be based purely on factors such as computation time.

An algorithm was created in Matlab to generate averaged strain images from the 3-D data matrix.

- Firstly, a pixel is chosen. The convolution is applied to the neutron intensity spectrum as a function of time of flight, the Bragg edges are found, and then a particular Bragg edge is chosen and 'zoomed in on'.
- The maximum of the convolution in the vicinity of this Bragg edge is found, and the time of flight point corresponding to this maximum is assigned to that particular pixel.
- This process is repeated for each pixel in the detector, until each pixel in the array has an assigned time of flight value corresponding to the particular Bragg edge.
- Conversions to average lattice spacing and average strain along that neutron path can then be carried out.

On the following page there is a flow chart demonstrating the method for the interpretation of the experimental data.

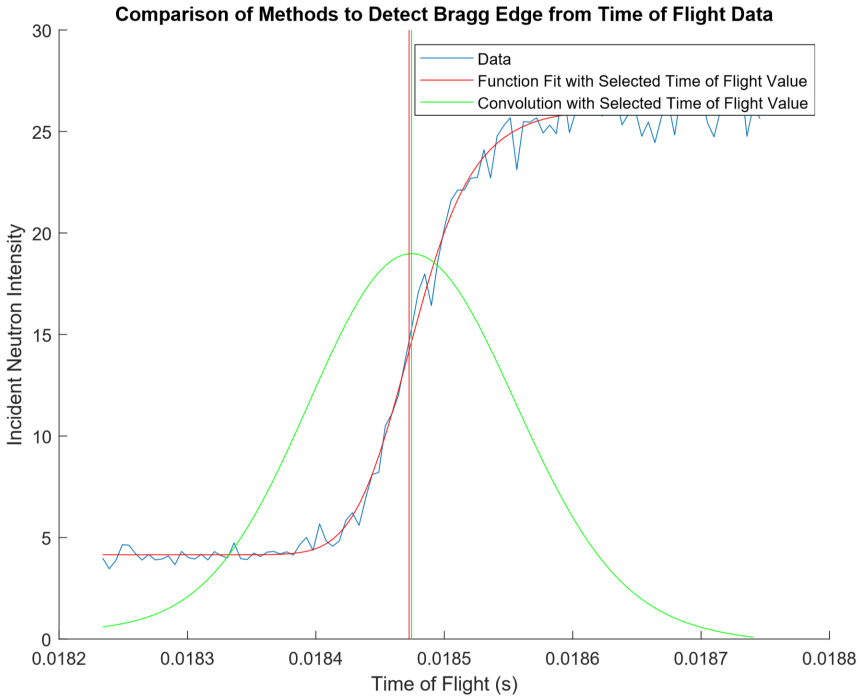

Figure 7: Comparison of methods to pick out Bragg edge centre

The fit of Equation 4 (red) to the neutron transmission data (blue) at a Bragg edge is shown in Figure 7. The convolution applied to the data (green) is also displayed, and the centre of the Bragg edge, as detected by each method, is shown. They are seen to be very similar in position, and in fact only differ by less than the width of a time of flight bin, less than the uncertainty associated with the Bragg edge centre detection. This provides some evidence that the convolution method is accurate in its detection of the centre of Bragg edges.

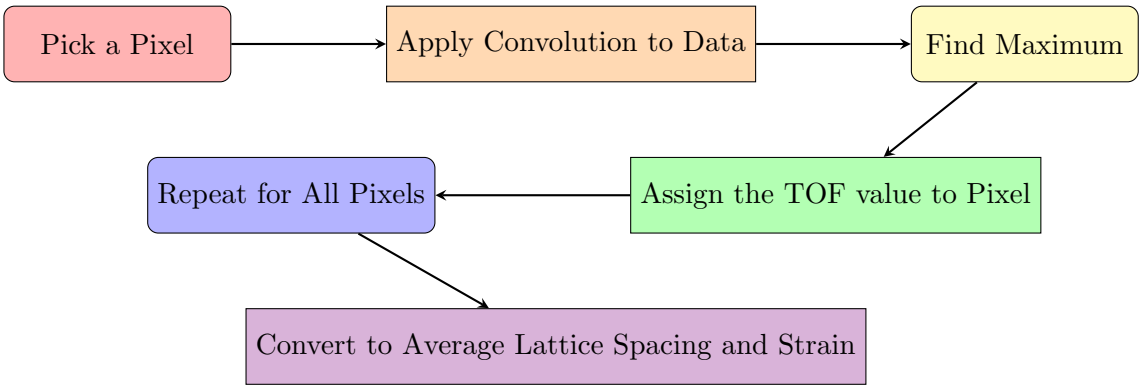

The convolution method was then used to create images from the data, by detecting the centre of a chosen Bragg edge for each pixel using the convolution, and then assigning this value to the relevant pixel, as described in the flow chart above.

5 Results and Discussion

Firstly, the data obtained from imaging the unstrained polycrystalline sample was analysed using the method outlined above.

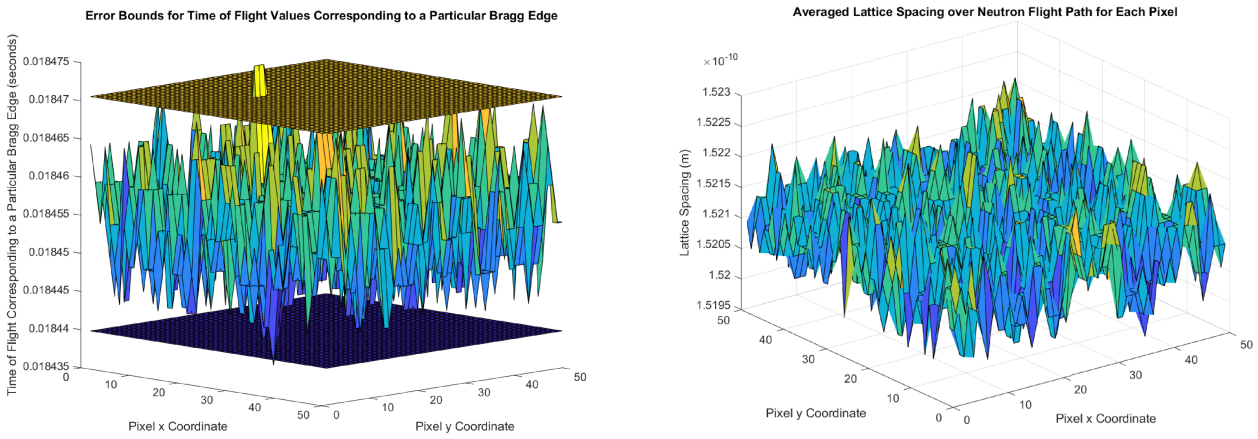

Figure 8: Left - Time of flight values corresponding to a particular Bragg edge for the unstrained sample data with uncertainty bounds. Right - 'Average' lattice spacing along neutron beam flight path for each pixel

The plot on the left of Figure 8 shows the time of flight values corresponding to the Bragg edge being examined for each pixel in the detector array. While there appears to be significant variation in the Bragg edge position across the pixels, indicating varying strain through the sample, the uncertainty bounds represented by the upper (yellow) and lower (blue) planes show that this variation is very small, mostly contained within the uncertainty bounds associated with the convolution method. This supports the idea that this sample has very little strain present inside.

On the right of Figure 8 is a plot of the average lattice plane spacing corresponding to the particular Bragg edge being analysed along each neutron beam path corresponding to each pixel. The time of flight values associated with the Bragg edge for each pixel have been converted to lattice spacing values using Equation 5 to produce this plot. Since it is of an unstrained sample, the unstrained lattice plane spacing, d_0, corresponding to this particular plane present in the polycrystalline material can be determined by averaging over the lattice spacing values for each pixel in this plot.

This value for d_0 can then be utilised to calculate the strain present in another sample.

These images were constructed using the same method; however, this data corresponds to a strained sample. The strain does not vary in the x direction of this cross section, see left plot of Figure 9.

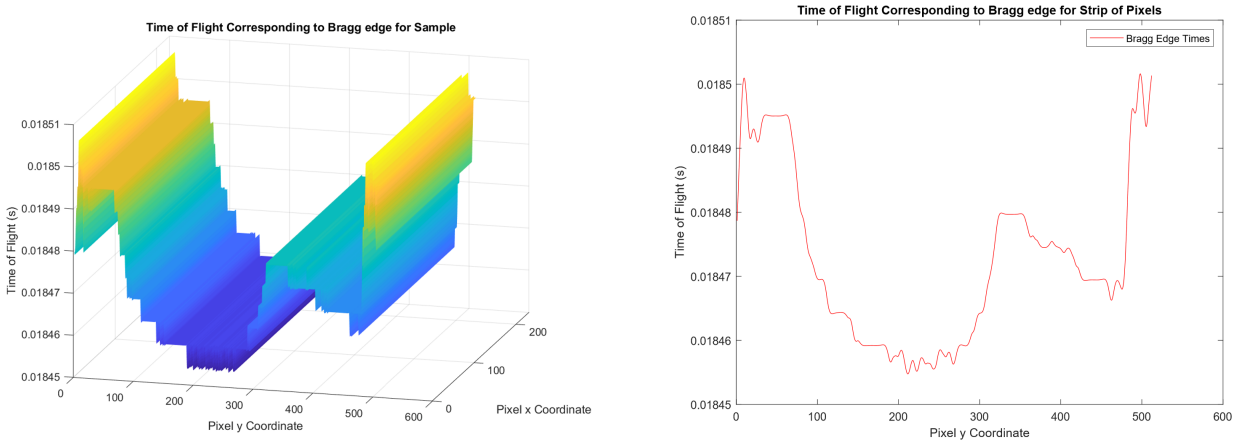

Figure 9: Left - Time of flight values corresponding to a particular Bragg edge for the strained sample data. Right - Variance of Bragg edge position along pixel y axis

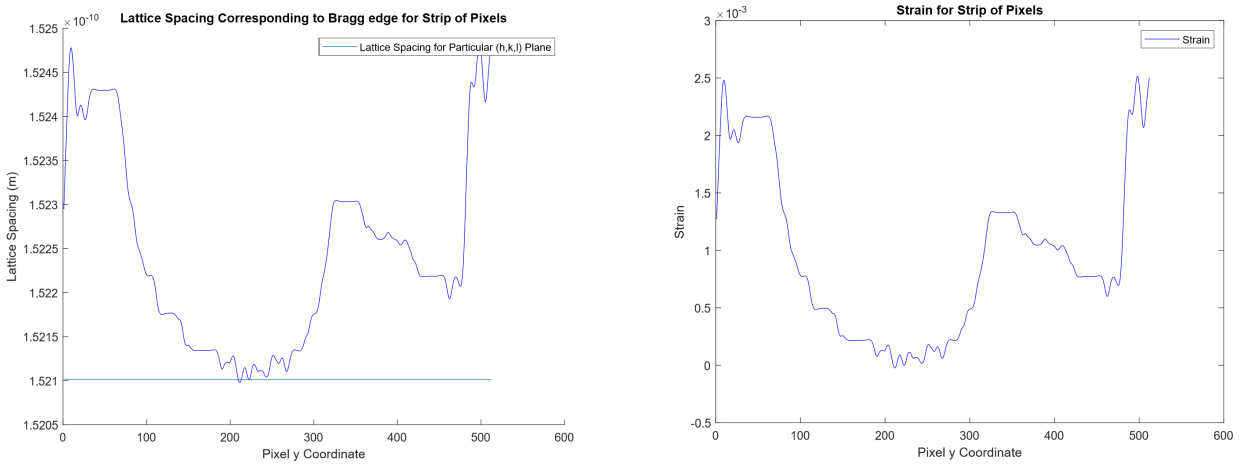

Figure 10: Left - Average lattice spacing for each pixel from the strained sample data with the unstrained spacing, d_0, displayed. Right - Average strain along each flight path for each pixel y coordinate.

On the left side of Figure 10, the unstrained lattice spacing is displayed as a flat line, calculated using the unstrained sample, along with the average lattice spacing for each pixel for the strained sample. Using this information, the average strain along each neutron flight path corresponding to each pixel was calculated using $\varepsilon = \frac{d-d_0}{d_0}$, and is displayed in the right plot of Figure 10.

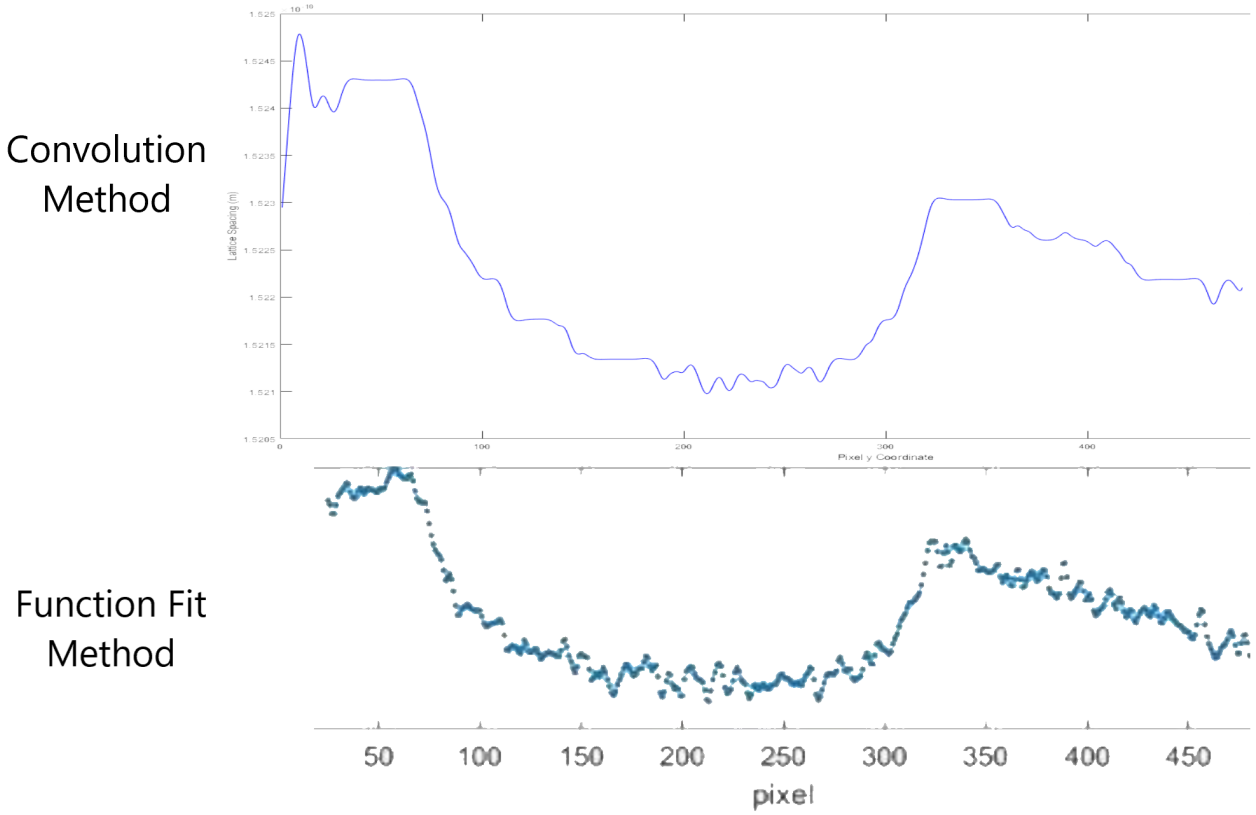

Figure 11: Comparison of methods for determining average lattice spacing along neutron beam flight path for each pixel from the strained data sample.

A comparison between the generated average lattice spacing images using the convolution and function fit methods for the strained sample data is provided in Figure 11. The similarity between the plots reinforces the validity of the convolution method, as it appears to closely mimic the output of the established function fit method.

Using the convolution method to detect the position of Bragg edges in the neutron intensity data for each pixel, average-strain-along-neutron-path cross sectional images can be produced, and in conjunction with the knowledge that strains along the neutron path contribute to the average strain in accordance with the longitudinal ray transform, it may be possible, in some cases, to reconstruct the strain tensor field throughout an imaged polycrystalline material. This has already been achieved for some special cases, and it is reasonable to assume that in the future this technique could be used to carry out non-destructive analysis in many material testing applications.

References

[1] Santisteban, J.R. et. al 2001, 'Strain imaging by Bragg edge neutron transmission', *Nuclear Instruments and Methods in Physics Research A 481 pp. 765–768*

[2] Josic, L., Steuwer, A., Lehmann, E. 2010, 'Energy selective neutron radiography in material research', *Appl Phys A (2010) 99: pp. 515–522*

[3] Woracek, R. et. al 2015, 'Neutron Bragg edge tomography for phase mapping', *Physics Procedia 69 (2015) pp. 227–236*

[4] De Broglie, L. 1923, 'Waves and Quanta', *Nature 112, 540*

[5] Bragg, W.H., Bragg, W.L. 1913, 'The Reflection of X-rays by Crystals', *Proceedings of the Royal Society A - Mathematical, Physical and Engineering Sciences vol. 88, no. 605, pp. 428–438*

[6] Boin, M. 2011, 'Developments towards the tomographic imaging of local crystallographic structures', *The Open University, Milton Keynes*

[7] Davisson, C., Germer, L.H. 1927, 'Diffraction of Electrons by a Crystal of Nickel', *Physical Review vol. 30*

[8] Einstein, A. 1905, 'On the Electrodynamics of Moving Bodies', *Annalen der Physik 17 (1905) pp. 891-921*

[9] Wensrich, C.M. et. al 2016, 'Bragg-edge neutron transmission strain tomography for in situ loadings', *Nuclear Instruments and Methods in Physics Research B 383 (2016) pp. 52–58*